

Helicopter Health Monitoring Using an Adaptive Estimator



Jonathan Alkahe
Graduate Student



Omri Rand
Professor



Yaakov Oshman
Associate Professor

Faculty of Aerospace Engineering
Technion—Israel Institute of Technology, Haifa 32000, Israel

A new health and usage monitoring methodology for detection and identification of damage in a helicopter rotor is presented. A full-scale rotor analysis in forward flight has been carried out using a detailed model of the coupled blade-fuselage behavior. Several rotor component faults, as well as local blade stiffness defects are considered. A set of Kalman filters is constructed, where the calculated blade tip response, in addition to elastic modes, comprises a state vector. In the proposed approach, each filter is based on the assumption that a particular fault has occurred. The best fitting model, according to measurements taken from the truth model, is determined in a probabilistic manner. In the numerical study used to demonstrate the performance of the method, two sets of noisy measurements are generated. The first set is based on blade tip sensors, and the second set consists of non-rotating hub loads. A Monte-Carlo analysis followed by a statistical experiment enables a comprehensive view of the statistical nature of the results. A parametric study is presented and conclusions concerning the detectability of damage in a helicopter rotor and the efficiency of the proposed method are drawn.

Introduction

The detection of damage as a part of self health and usage monitoring system (HUMS) in structural systems is an important contributor to their safety, reliability and structural integrity. Early damage detection has the potential of reducing life cycle costs and increasing replacement time intervals. If damage is located and monitored, then components of the structure may be replaced before a critical point is reached and a dangerous failure occurs. Particularly, the components of a helicopter rotor are subjected to high periodic loads and expected to perform under harsh environmental conditions. These factors, combined with the absence of redundant load paths, frequently result in early replacement of structural components, therefore causing an increase in maintenance costs.

One class of damage detection methods in which damage is seen as a change in the parameters of a structural model is based on modal information (Refs. 1–7). Typically, modal-based damage detection methods use a finite element model of the system combined with experimental modal data to determine damage location and extent. The effect of cracks on the natural frequencies of a cantilever beam is demonstrated in Refs. 3–4. These cracks were modeled using rotational springs with equivalent stiffness. Since natural frequencies change very slightly as crack size and location varies, the addition of noise, not treated in these studies, would significantly decrease the identification capability.

In Ref. 5 the changes in mode shape due to the presence of structural damage were determined. A finite element model with a reduction of the modulus of elasticity in a prescribed segment was implemented. It was shown that the elastic rotation undergoes a step jump in value when crossing the damage location, while the displacement parameter takes a change in its slope.

An eigenstructure assignment technique for damage detection in rotating structures is demonstrated in Ref. 6. The damage is simulated by a 10% loss of mass and stiffness in the damaged element. A test case with noise contaminated mode shapes is also presented. An extension of this algorithm for rotating helicopter blades accounting for hovering aerodynamics is presented in Ref. 7. The blade's aerodynamics is incorporated as a damping term in the structural dynamics of the blade. The damage is shown to be properly characterized when flapping modes are used. However, the algorithm presented is based on a least-squares estimation procedure which might be inaccurate in some cases.

Another approach for damage detection in beam structures described in the literature uses a subspace rotation algorithm (Ref. 2). This method views damage location and damage extent as two different problems requiring two separate solutions. In this approach, damage is manifested as changes in the mass, damping and stiffness matrices of the structure. Strain sensors were used, therefore, a method for extracting displacement frequency responses from strain data was presented. This study shows that higher-order vibration modes are required to locate damage events. In addition, condensation methods can not be used to remove rotational degrees of freedom because of their strong coupling with translation degrees of freedom.

Several studies, in addition to Ref. 7, have been published concerning damage detection in helicopters (Refs. 8–11). In these works, a model of a rotor combined with a rigid fuselage is utilized to simulate typical main rotor components faults. The model results are then inserted as inputs to a neural network in order to complete the training stage. The network's detection capability is demonstrated using another set of a priori calculated model results (validation data), and is tested in several cases including noise corrupted inputs. The results shown in these studies indicate that for a network trained on ideal data alone, miss-identification begins even in the presence of low levels of noise (as low as 2%) in the validation data. However, the network trained on noisy data generates no classification error for noise less than 10% and relatively small error

Presented at the American Helicopter Society 57th Annual Forum, Washington, D.C., May 9–11, 2001. Manuscript received October 2001; accepted May 2003.

at even higher noise levels. The results also demonstrate that good performance is achieved for relatively large damage levels (for example, an approximately 20% pitch link stiffness reduction). This emphasizes the importance of training the neural network using noisy data. The main drawback of the noisy input training procedure is the large amount of data needed to appropriately handle the stochastic nature of these inputs. This method also lacks the flexibility to easily accommodate a change in helicopter model parameters (i.e., c.g. locations, moments of inertia, aerodynamic coefficient changes, etc.) after the training stage.

In Ref. 12 a coupled elastic rotor-fuselage helicopter model is presented and its results are compared with flight test data. The analysis is based on fuselage vibration measurements. All of the faults considered in this work were found to increase the 1/rev vibration. The analysis was able to capture the trend of vibration amplitude, however, the phasing of the vibration was not predicted accurately. Moreover, a fault detection methodology is not described in the above study.

The current status of HUMS is reviewed in Refs. 13–17. Via an analysis of its vibration diagnostic capabilities, Ref. 13 shows HUMS to be an effective maintenance tool. A wide range of faults of gearboxes, shafts, bearings and tail rotors have been detected using vibration monitoring.

The HUMS described in Ref. 14 is composed of two major components. The first is the on-board system, which provides rotor trim and balance, drive train monitoring and engine checks. These functions are based on vibration measurements. The second component is the ground station, which provides diagnostic/prognostic and maintenance requirements. The validation of the open system approach (Ref. 14) is described in Ref. 15. Five modules from a diverse set of manufacturers compose the system.

A comparison of aircraft usage based on the original predicted flight spectrum and a HUMS measured aircraft usage is described in Ref. 16. In this work a ground-based system is described and utilized. Overall, results indicate an increase in component life based on HUMS, although torsional fatigue load components resulted in a decreased life time. In addition, a small cost benefit is also gained.

A composite flexbeam as a part of a rotor system is investigated in detail in Ref. 17. Piezoceramic sensors are placed on the top and bottom surfaces. Various damage detection methods are compared.

In the present study, the damage detection methodology is based on the multiple-model adaptive estimation (MMAE) approach. This algorithm, as opposed to other published methods, treats process and measurement noise inherently, and, therefore, is more suitable to account for the modeling errors and noisy environment of a helicopter rotor. In the MMAE method various rotor component faults and levels are considered, where each case is adequately represented by a finite element model. A Kalman filter is tuned according to each model and the best fitting one is determined in a probabilistic manner based on noisy measurements. Since the MMAE approach is inherently model-based, it is, like all model-based methods, sensitive to the fidelity of the mathematical model used. However, as a preliminary study shows, (Ref. 18) this sensitivity can be handled quite effectively using process noise compensation within the Kalman filters comprising the MMAE filter bank.

Previous studies concerning a rotating blade and a fixed shaft rotor in vacuum have been reported in Ref. 19. Results have clearly demonstrated high damage detection and identification capability. In addition, an extensive parametric study was carried out, giving insight on the influence of various parameters. Crack detection in helicopter main rotor elastic blades, including aerodynamic effects, is discussed in Ref. 20. Results indicate that detecting a local stiffness defect, representing a crack, using blade tip response measurements, is very difficult due to the small changes between the damaged and undamaged models. However, a well designed statistical experiment enables high detection probabilities combined with low false alarm rates. Rotor component fault identification is

discussed in Ref. 21. Various sensor and fault types are considered, and the performance of the proposed approach is presented.

In this paper, a fixed-shaft helicopter rotor, as well as the case of a free, trimmed forward flight are discussed. Several faults are introduced using a detailed analytical model of the helicopter. Various sensor types are utilized including measurement noise. The proposed algorithm performance is demonstrated, combined with useful suggestions to overcome some damage detection difficulties. This approach eliminates the need for a training stage, which characterizes FDI (Fault Detection and Identification) algorithms based on neural networks. Two additional important features of the proposed approach are 1) inherent treatment of process noise, which facilitates handling unmodeled inputs and model parameter uncertainties, and 2) statistically optimal filtering of measurement noise, that turns out to be much more efficient than commonly used averaging techniques. Each one of the filters is based on a model of the dynamic system. This contributes to the flexibility of the algorithm, by allowing to perform frequent changes and updates in the models. Another key advantage of the proposed FDI algorithm is the judgment and decision making process, which is optionally left to the human operator, due to the probabilistic nature of the results.

The paper is organized as follows. The next section describes in detail the adaptive estimator algorithm adopted for fault detection and identification. This is followed by a brief description of the development of the helicopter structural model. The results of an extensive simulation study are then presented. First, the case of a fixed-shaft rotor with component faults is introduced. The proposed algorithm capabilities are discussed for several sensor types and measurement noise levels. This is followed by a forward flight analysis, where rotor component faults are identified using fuselage vibration sensors. Then, the case of a local stiffness defect in elastic blades is discussed. Finally, conclusions concerning the efficiency and robustness of the proposed approach are drawn.

Multiple-Model Adaptive Estimation

In various estimation problems, specifically in damage detection cases, uncertain parameters exist within the system model used for algorithm design. Typically, these parameters can undergo large jump changes. Such problems give rise to the need for estimation of parameter values simultaneously with estimation of state variables. One means of accomplishing this is the multiple model adaptive estimation technique (Refs. 22, 23). The system is assumed to be adequately representable by a linear stochastic state model, with uncertain parameters affecting the matrices defining the structure of the model or the noise distribution model. It is further assumed that the parameters can take only discrete values. When the parameters belong to a continuous space, discrete representative values have to be chosen within this parameter space. A Kalman filter is then designed for each choice of parameter value, resulting in a bank of K separate filters. Based on the residuals of each one of these K filters, the conditional probabilities of each discrete parameter value being “correct” (given the measurement history to that time) are evaluated recursively. This procedure is summarized in Fig. 1.

Following the development presented in Refs. 23 and 24, consider the system model described by the first-order, linear, stochastic differential state equation of the form

$$\dot{\mathbf{x}}(t) = \mathbf{F}(\mathbf{a}, t)\mathbf{x}(t) + \mathbf{G}(\mathbf{a}, t)\mathbf{w}(t) + \mathbf{B}(\mathbf{a}, t)\mathbf{u}(t), \quad (1)$$

with noisy measurements described by the discrete time equation

$$\mathbf{z}_k = \mathbf{H}_k(\mathbf{a})\mathbf{x}_k + \mathbf{v}_k \quad (2)$$

where $\mathbf{x}(t)$ is the system state vector and $\mathbf{u}(t)$ is the control vector. \mathbf{x}_k and \mathbf{z}_k are the state and measurement vectors at the discrete time t_k ,

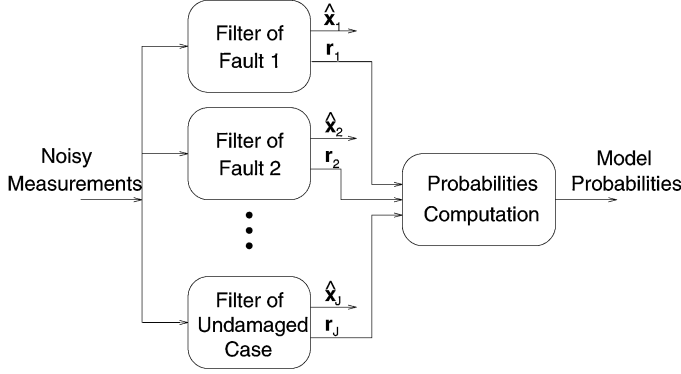


Fig. 1. The MMAE procedure.

respectively. It is assumed that the process noise vector, $\mathbf{w}(t)$, and the discrete measurement noise vector, \mathbf{v}_k , are independent, zero-mean, white Gaussian noise processes with covariances

$$\mathbb{E}\{\mathbf{w}(t)\mathbf{w}^T(s)\} = \mathbf{Q}(t)\delta(t - s) \quad (3)$$

and

$$\mathbb{E}\{\mathbf{v}(t_i)\mathbf{v}^T(t_j)\} = \mathbf{R}(t_i)\delta_{ij}, \quad (4)$$

where δ_{ij} is Kronecker's delta function. Moreover, \mathbf{a} is a vector containing the structural damage effects, $\mathbf{F}(\mathbf{a}, t)$ is the dynamics matrix, $\mathbf{G}(\mathbf{a}, t)$ is the process noise distribution model, $\mathbf{B}(\mathbf{a}, t)$ is the control matrix and $\mathbf{H}_k(\mathbf{a})$ is the measurement matrix at time t_k . In the case of a discrete stochastic state propagation model, Eq. (1) is replaced by the following equation:

$$\mathbf{x}_{k+1} = \Phi_{k+1,k}(\mathbf{a})\mathbf{x}_k + \mathbf{w}_{d,k} + \Psi_{k+1,k}(\mathbf{a})\mathbf{u}_k. \quad (5)$$

Assuming that the dynamic system is quasi-stationary, the following relations hold:

$$\Phi_{k+1,k}(\mathbf{a}) = e^{\mathbf{F}_k(\mathbf{a})\Delta t} \quad (6)$$

$$\Psi_{k+1,k}(\mathbf{a}) = \mathbf{B}_k(\mathbf{a})\Delta t, \quad (7)$$

where Δt is the discretization time interval. In Eq. (5), $\mathbf{w}_{d,k}$ is the equivalent discrete time process noise vector with the covariance

$$\mathbb{E}\{\mathbf{w}_d(t_i)\mathbf{w}_d^T(t_j)\} = \mathbf{Q}_d(t_i)\delta_{ij} \quad (8)$$

where $\mathbf{Q}_d(t_i)$ is calculated using the relation

$$\mathbf{Q}_d(t_i) = \mathbf{G}_k\mathbf{Q}_k\mathbf{G}_k^T\Delta t. \quad (9)$$

Since \mathbf{a} may assume a continuous range of values over the space of allowable parameters, it is necessary to discretize \mathbf{a} into a set of J vector values: $\mathbf{a}_1, \mathbf{a}_2, \dots, \mathbf{a}_J$. A multiple model adaptive estimator consists of J independent Kalman filters, in which the j th filter is constructed according to a specific parameter value \mathbf{a}_j . These J filters form a bank of elemental filters which are processed in parallel. Each elemental filter produces its own estimate of the true state, denoted as $\hat{\mathbf{x}}_j(t_i)$, for the j th hypothesized value of \mathbf{a} . The residuals of all J elemental filters are then used to calculate the probability that \mathbf{a} assumes the value \mathbf{a}_j at time t_i , for $j = 1, 2, \dots, J$. This probability is called the ‘‘hypothesis conditional probability’’ and is denoted as $p_j(t_i)$. This conditional probability represents the validity of the j th filter's system model at time t_i . The hypothesis conditional probabilities $p_j(t_i)$, $j = 1, 2, \dots, J$, are calculated at each sample time t_i , by the recursive equation

$$p_j(t_i) = \frac{f_{\mathbf{z}(t_i)|\mathbf{a}, \mathbf{Z}(t_{i-1})}(\mathbf{z}_i|\mathbf{a}_j, \mathbf{Z}_{i-1})p_j(t_{i-1})}{\sum_{k=1}^J f_{\mathbf{z}(t_i)|\mathbf{a}, \mathbf{Z}(t_{i-1})}(\mathbf{z}_i|\mathbf{a}_k, \mathbf{Z}_{i-1})p_k(t_{i-1})} \quad (10)$$

where \mathbf{Z}_{i-1} is the measurement history from the first sample time until sample time t_{i-1} , and

$$f_{\mathbf{z}(t_i)|\mathbf{a}, \mathbf{Z}(t_{i-1})}(\mathbf{z}_i|\mathbf{a}_j, \mathbf{Z}_{i-1}) = \frac{1}{(2\pi)^{S/2}|\mathbf{A}_j(t_i)|^{1/2}} \exp\left\{-\frac{1}{2}\mathbf{r}_j^T(t_i)\mathbf{A}_j^{-1}(t_i)\mathbf{r}_j(t_i)\right\} \quad (11)$$

where S is the number of sensors. The j th filter residual vector is

$$\mathbf{r}_j(t_i) = \mathbf{z}(t_i) - \mathbf{H}_j(t_i)\hat{\mathbf{x}}_j(t_i^-), \quad (12)$$

where $\hat{\mathbf{x}}_j(t_i^-)$ is the j th filter-predicted state estimate. The j th filter-computed residual covariance matrix, $\mathbf{A}_j(t_i)$, is calculated as

$$\mathbf{A}_j(t_i) = \mathbf{H}_j(t_i)\mathbf{P}_j(t_i^-)\mathbf{H}_j^T(t_i) + \mathbf{R}_j(t_i), \quad (13)$$

where $\mathbf{P}_j(t_i^-)$ is the j th filter prediction error covariance. The residual of the j th filter plays a major role in determining $p_j(t_i)$. As is evident from Eq. (10), the filter with the smallest value of $\mathbf{r}_j^T(t_i)\mathbf{A}_j^{-1}(t_i)\mathbf{r}_j(t_i)$ assumes the largest conditional hypothesis probability. Thus, this algorithm is consistent with the intuition that the residuals of a well-matched filter should be smaller (relative to the filter's internally computed residual covariance, \mathbf{A}_j) than the residuals of a mismatched filter. To allow the estimator to adapt to the changing parameter value, the hypothesis conditional probabilities are artificially bounded below by a small number, taken in this study to be 0.0005. This ensures preventing any of them from converging to zero, which would make it very difficult for them to change significantly in response to a subsequent change in true parameter value.

Structural Model

The full-scale rotor analysis has been carried out using the software package RAPID (Ref. 25), which is capable of modeling general rotorcraft configurations, conventional helicopters and tilt-rotors. RAPID may handle nonuniform and dissimilar blades and is therefore suitable to the current task. Both rigid and elastic blade analyses are possible. Blade elasticity is modeled using a built-in model based analysis for structurally pretwisted spars. This analysis enables including the blade's axial, lead-lag, flap and twist elastic deformations, designated by u , v , w and ϕ , respectively. The model also includes fully articulated blades with arbitrary pitch, flap and lag offsets, root springs and dampers, and a detailed control system mechanism (swashplate, elastic pitch links, pitch horn, etc.), which enables a study of faults in these components.

The package RAPID enables a nonlinear solution of the helicopter equations of motion, derived with symbolic exactness. When convergence is achieved, the small perturbation equations are generated around a working point (or trim state). The global periodic mass, damping and stiffness matrices, denoted $\mathbf{M}(\mathbf{a}, t)$, $\mathbf{C}(\mathbf{a}, t)$ and $\mathbf{K}(\mathbf{a}, t)$, respectively, combined with the transformation to a first-order state equation, are used to construct the continuous dynamics matrix, $\mathbf{F}(\mathbf{a}, t)$ (see Eq. (1)) as follows:

$$\mathbf{F}(\mathbf{a}, t) = \begin{bmatrix} \mathbf{0} & \mathbf{I} \\ -\mathbf{M}(\mathbf{a}, t)^{-1}\mathbf{K}(\mathbf{a}, t) & -\mathbf{M}(\mathbf{a}, t)^{-1}\mathbf{C}(\mathbf{a}, t) \end{bmatrix}. \quad (14)$$

The control matrix $\mathbf{B}(\mathbf{a}, t)$ is given by

$$\mathbf{B}(\mathbf{a}, t) = \begin{bmatrix} \mathbf{0} & \mathbf{0} \\ \mathbf{0} & -\mathbf{M}^{-1} \end{bmatrix}. \quad (15)$$

In this work it is assumed that only one fault occurs. For the case of rigid articulated blades, the following component faults are investigated:

pitch-link damage, lag damper defect, friction in pitch bearing and moisture absorption. The case of a local damage in hingeless elastic blades is also considered. The damage detection algorithm consists of 5 different models running in parallel: four damaged rotor models, along with the baseline undamaged one.

Damage Identification Logic

The fault detection and identification (FDI) process is carried out during 5 rotor revolutions (approximately 1 sec) in which all the 5 models run in parallel. Detection based on a 5-rev. time interval, designated as t_p , is termed, in this study, single-run detection process. The decision logic is based on calculating the fitness probability for each of the models over an inspection time interval (designated as t_d), which includes only the last revolution. Let $p_j(t_i)$ denote the hypothesis conditional probability of the j th model at a discrete time t_i , and q_j refer to the fitness probability of the j th model. Then

$$q_j = \frac{\sum_{t \in t_d} p_j(t)}{\sum_{k=1}^J \sum_{t \in t_d} p_k(t)}. \quad (16)$$

Let q_{max} be defined as

$$q_{max} \triangleq \max_{j \in \{1, 2, \dots, J\}} \{q_j\}. \quad (17)$$

The model associated with q_{max} is said to describe the true damaged behavior in the best manner.

In order to provide a better view of the statistical nature of the results, a Monte-Carlo analysis (Ref. 26) is carried out, where the same damaged case is repeated, however with different noise values. The Monte-Carlo procedure continues until the identification probability of the model, found to be the most fitting, converges. In any case, an upper limit of 150 Monte-Carlo runs is set. This procedure results in estimated probability values for the single-run process. When the true case is the case of no damage, the single-run false alarm rate, designated by p_{FA} , is calculated. Single-run detection and identification probabilities result for each one of the cases where a fault occurs. These probabilities are designated by p_D and p_I , respectively.

Control of Error Probabilities

The overall false alarm and detection probabilities can be controlled using a well designed statistical experiment. Let H_0 and H_1 denote the hypotheses of "no damage" and "damage", respectively. Assume that N is the total number of single-run repetitions and n is the number of runs in which damage was detected. A decision criterion is defined as

$$n \underset{H_0}{\overset{H_1}{\gtrless}} n_D \quad (18)$$

where n_D is a predetermined threshold. When the true undamaged case is not detected, a false alarm results (type I error). The associated false alarm probability is calculated using the expression

$$P_{FA} \triangleq P(H_1|H_0) = \sum_{i=n_D}^N \binom{N}{i} p_{FA}^i (1 - p_{FA})^{N-i}. \quad (19)$$

When true damage is not detected, a missed detection (or type II error) occurs. The probability associated with this case is calculated as follows:

$$P_{MD} = 1 - P_D \triangleq P(H_0|H_1) = \sum_{i=1}^{n_D-1} \binom{N}{i} (1 - p_D)^i p_D^{N-i}. \quad (20)$$

A detector operating characteristics plot, showing P_D vs P_{FA} , can be constructed. Using this plot, the total number of runs and the threshold level can be tuned to achieve an overall low false alarm rate combined with a high detection probability, according to some specified requirements.

Simulation Study

An extensive numerical simulation study was carried out to analyze and demonstrate the performance of the proposed FDI method. In this study, various rotor component faults were investigated, using various kinds of measurements. For conciseness, not all simulation study results are presented herein. The interested reader is referred to Ref. 18 for a detailed description.

Tip response measurements

Consider a typical full-scale articulated two-bladed fixed-shaft rotor with rigid blades, whose properties are listed in Table 1. Forward flight conditions at advance ratio $\mu = 0.3$ were simulated including trim commands.

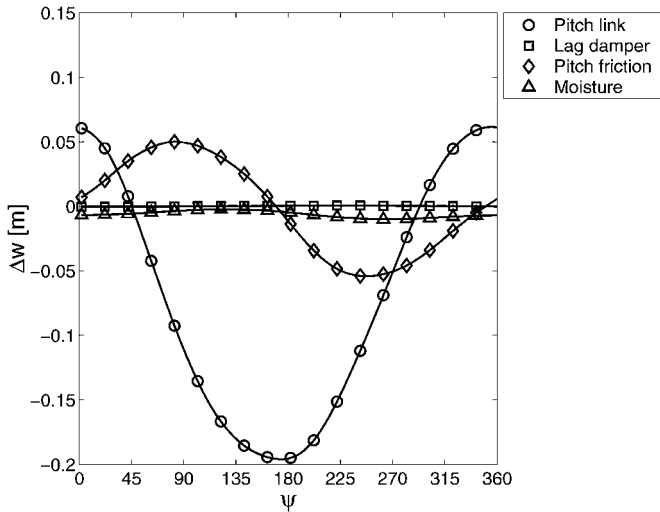
A parametric study was carried out, investigating the influence of various damage levels, for the faults mentioned in the previous section, combined with several noise levels. As mentioned above, only one fault may occur in one of the blades. Five damage levels were examined (except for the lag damper fault which has only 3 damage levels), each with five noise levels. The noise levels presented in the following figures are dimensional, where displacement noise is measured in meters and pitch angle noise is measured in radians. The measurements taken are tip response of the two blades (tip flap and lead-lag displacements along with the tip pitch angle).

Pitch link damage is manifested as a stiffness reduction caused by a crack. The damage spectrum includes five levels which vary from 10% stiffness reduction to 30%. Lag damper damage is modeled by reducing the damping coefficient by 50%, 60% and 68% (lead-lag stability margin). Pitch bearing friction is modeled by an increase in the pitch damping coefficient at the blade root. Five levels are considered: an increase by a factor of 4 up to a factor of 8. Moisture absorption (for the case of a composite blade) is manifested by an increase in the blade mass per unit length, from 2% mass increase up to 4% (five levels).

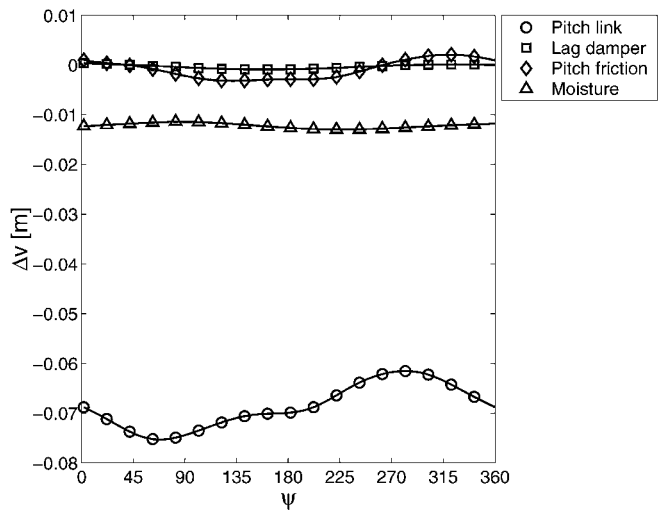
The performance of any FDI algorithm is based on differences between the various damaged cases under consideration. These differences are usually manifested in the matrices defining the dynamic response of the system (the mass, damping and stiffness matrices). Incipient structural faults cause small changes to appear in several components of the system's dynamic matrices, therefore, producing a slightly different structural response—known as the fault signature. Most of the FDI methods exploit these signatures for damage detection and identification. When using a filtering algorithm, as described in this work, the changes in the system matrices transform to differences in the dynamics matrix $\mathbf{F}(\mathbf{a})$, as

Table 1. Rotor properties

Parameter	Value
Radius	7.1 m
Chord	0.76 m
Blade twist angle	-9°
Baseline pitch link stiffness	10 ⁶ N/m
Baseline lead-lag damper	3000 N-m-s
Baseline pitch damper	10 N-m-s
Mass per unit length	20 Kg/m
Angular velocity	34 rad/s



(a) Tip flap differences Δw

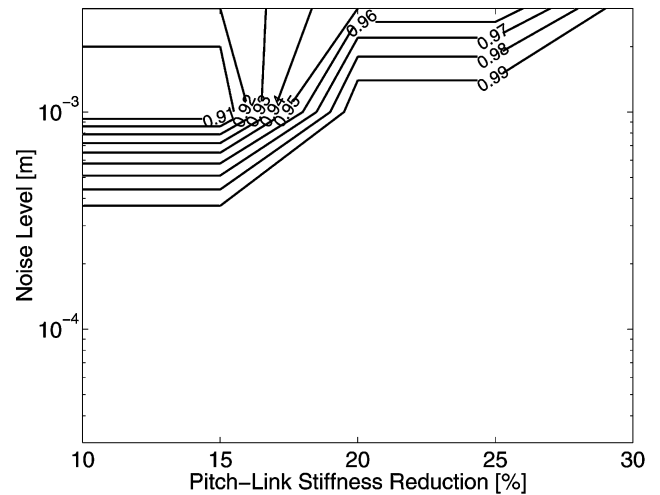


(b) Tip lead-lag differences Δv

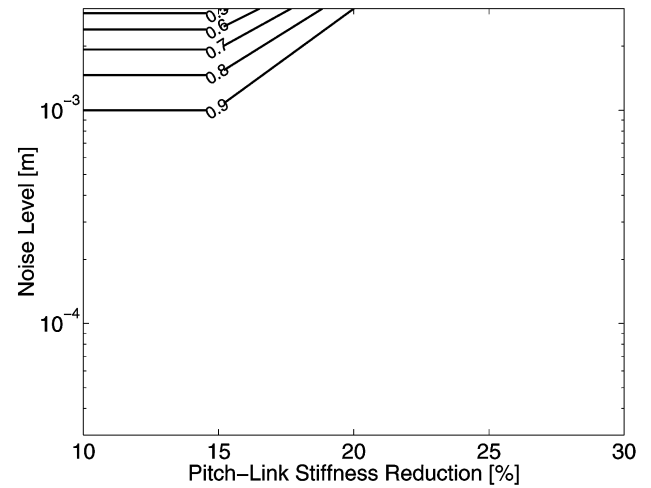
Fig. 2. Blade tip response differences.

discussed previously. An example of several fault signatures, treated as measurement differences, is presented in Fig. 2. The tip flap displacement difference is shown in Fig. 2(a), and Fig. 2(b) shows the lead-lag displacement differences. The differences are calculated for all damaged models with respect to the baseline undamaged tip response. Clearly, pitch-link damage results in a relatively large response difference and is, therefore, expected to be highly detectable. However, the lag damper damage causes hardly any difference in the observables, suggesting detection difficulties.

Figures 3–6 show the single-run probability contours, estimated using a Monte-Carlo analysis consisting of a maximum of 150 runs. Figure 3 presents the detection and identification probability contours for a pitch link fault, respectively. The relatively high probability values indicate that this fault is highly detectable and identifiable. Moreover, a low noise level combined with a high damage level produce better detection and identification results, as can be expected. An interesting phenomenon is revealed where the detection probability decreases as the noise level increases, until a certain point where the former starts to increase. The reason is that for high noise levels, the differences between the models are masked by the noise, rendering similar probabilities (around 0.2) to all the models. Therefore, the detection probability, consisting of the



(a) Detection probability



(b) Identification probability

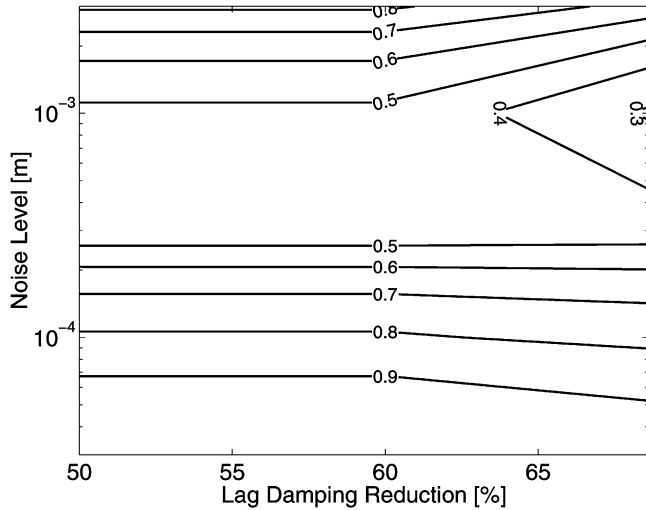
Fig. 3. Pitch link damage detection and identification performance.

probability sum of all 4 damaged models, tends to the theoretical value of approximately 0.8. This phenomenon is demonstrated in Figs. 4(a), 5(a) and in Fig. 6(a) as well.

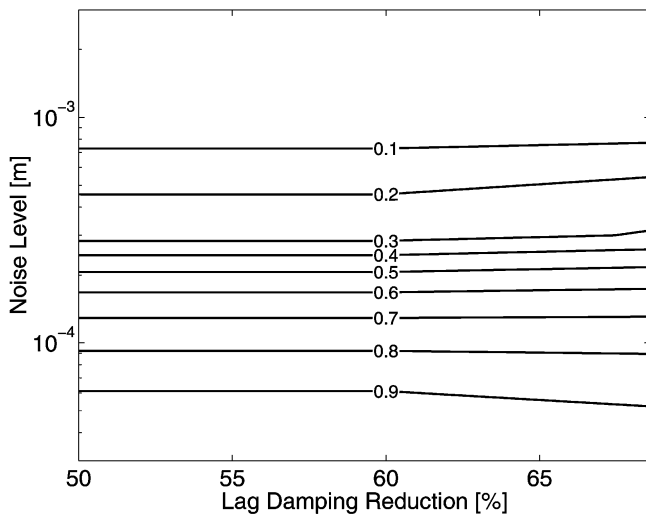
Figure 4 shows the probability contours for the lag damper damage. Clearly, this damage case is less detectable. As seen from the figures, the detection and identification probabilities are not sensitive to the damage level. This is because relatively small lag damping values exist even in the undamaged case. Figure 5 shows the probability contours for the pitch friction case. As shown, this fault is also relatively easy to detect and identify. Figure 6 shows the probability contours for the moisture absorption case. This type of fault is somewhat less detectable than the pitch link and pitch friction cases.

Figure 7 presents the false alarm rate contours. Since all 5 models are included, at each damage level, all 4 faulty models assume the corresponding damage value. For example damage level 1 means 10% pitch link stiffness reduction, 50% lag damping reduction, pitch friction increase of a factor of 4 and 2% mass increase due to moisture absorption. For high noise levels the false alarm probability approaches 0.8, as theoretical analysis predicts.

A statistical experiment composed of several repetitions of a single-run process enables some control on the overall false alarm and detection



(a) Detection probability

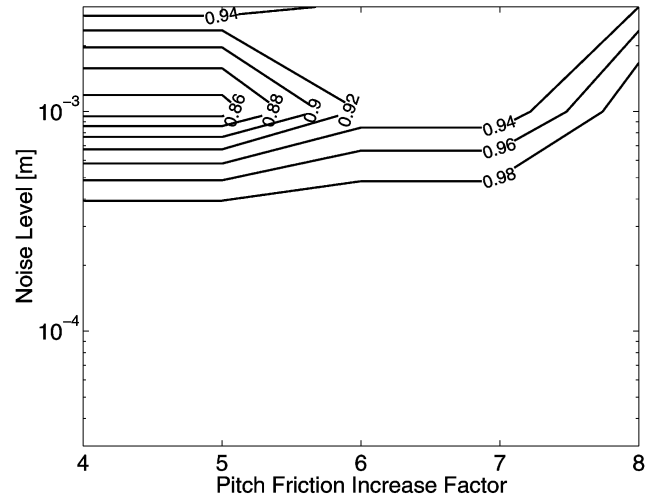


(b) Identification probability

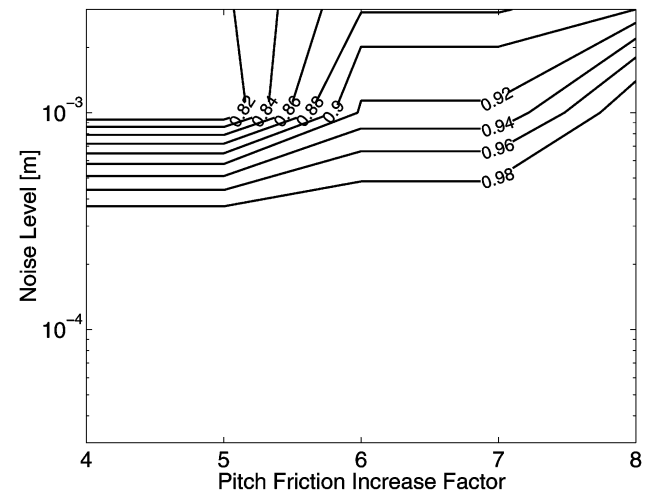
Fig. 4. Lag damper damage detection and identification performance.

probabilities. The results of such an experiment depend on the single-run value of p_{FA} and p_D , as discussed in the previous section. As an example, the case of lag damper damage (50% lag damping reduction) is considered. In this case, in order to achieve reasonable single-run false alarm and detection probabilities, only a very low noise level is allowed. Figure 8 shows two examples: in the first case, shown in Fig. 8(a), a low noise level ($\sigma = 10^{-4}$ m) is considered, and the single-run probabilities, p_{FA} and p_D , assume the values 0.1 and 0.8, respectively. Clearly, the number of repetitions (N) needed for low false alarm and high detection rates is not large ($N \approx 5$). For a higher noise level, where p_{FA} and p_D assume the unacceptable values of 0.4 and 0.5, respectively, as demonstrated in Fig. 8(b), a much larger number of runs is needed ($N \approx 400$), but, still, reasonable values of P_{FA} and P_D can be achieved.

Let the required overall false alarm and detection rates assume acceptable representative values of 0.05 and 0.95, respectively. Using the above statistical experiment, the number of repetitions (N) can also be presented as contours, for each fault under consideration. For example, the contour lines in Fig. 9 correspond to the smallest values of N required to meet those rates in the moisture absorption fault.



(a) Detection probability



(b) Identification probability

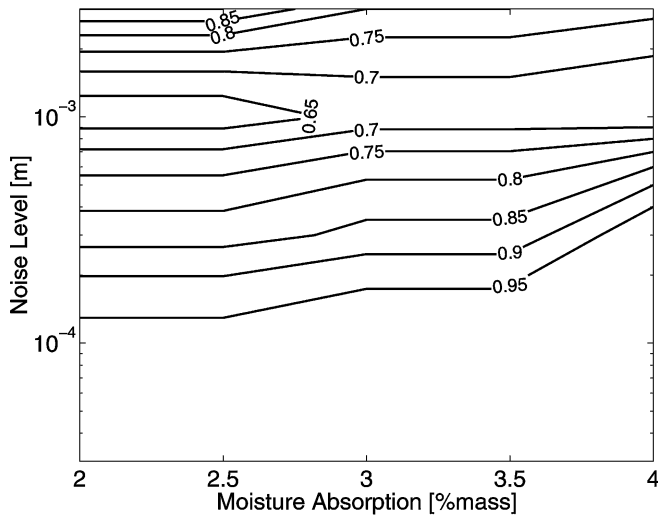
Fig. 5. Pitch friction detection and identification performance.

Non-rotating hub load measurements

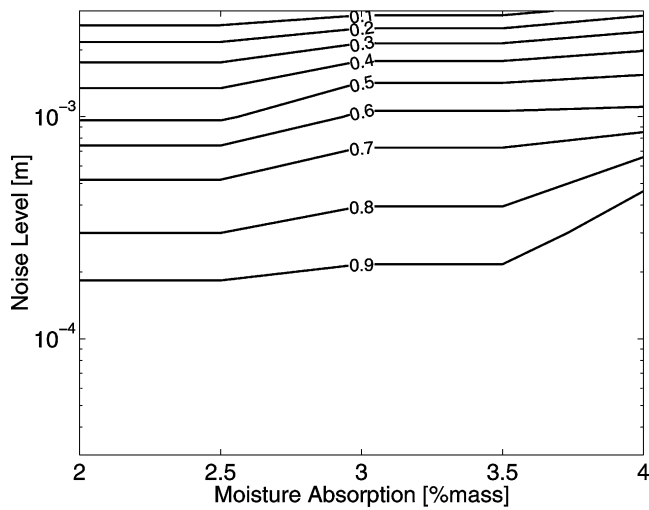
Consider the same rotor as in the previous section. In this case, only one damage level is considered, which consists of 5% stiffness reduction for the pitch link damage, 68% lag damping reduction, pitch friction which results in a pitch damping increase of factor 1.5, and 0.5% mass increase for the moisture absorption case. Note that all these damage levels are lower than the levels presented in the previous section. Moreover, a much higher measurement noise level is induced, with standard deviations of 1 KN and 1 KN-m for the force and moment measurements, respectively.

Fault signature examples, represented here as load differences of each of the damaged cases under consideration with respect to the undamaged case loads, are shown in Fig. 10. Figure 10(a) demonstrates the normalized hub force differences in the lateral direction (ΔF_y), and Fig. 10(b) shows the normalized pitching moment differences (ΔM_y). The moisture absorption case clearly results in larger differences, indicating high detectability. The other damage cases produce load differences bounded by $\pm 1\sigma$ of the noise.

The single-run identification probability time histories, for the various damage cases, are shown in Fig. 11. These results indicate that the model associated with the highest probability is indeed the correct one.

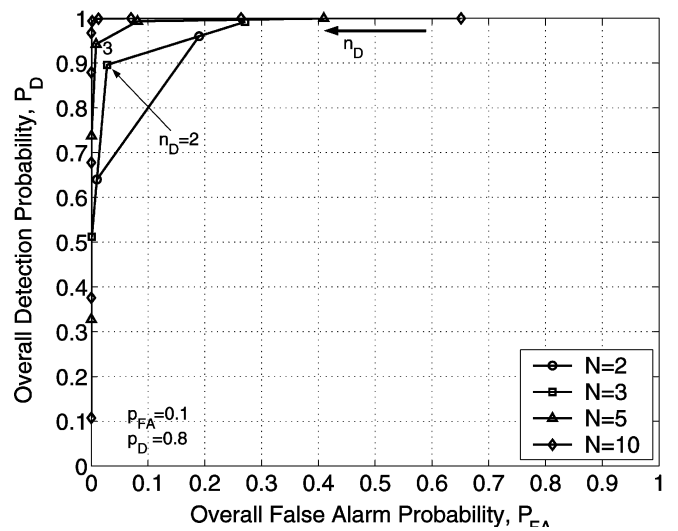


(a) Detection probability

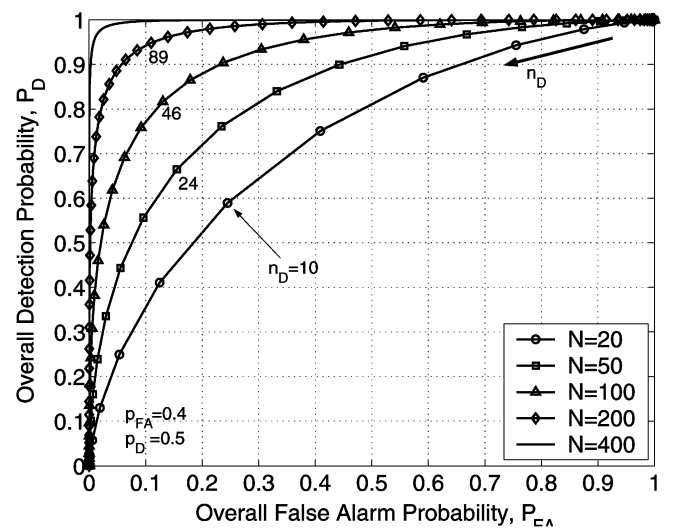


(b) Identification probability

Fig. 6. Moisture absorption detection and identification performance.



(a) Experiment results for a noise level of $\sigma = 10^{-4}$ m



(b) Experiment results for a noise level of $\sigma = 10^{-3}$ m

Fig. 8. Detector operating characteristics examples.

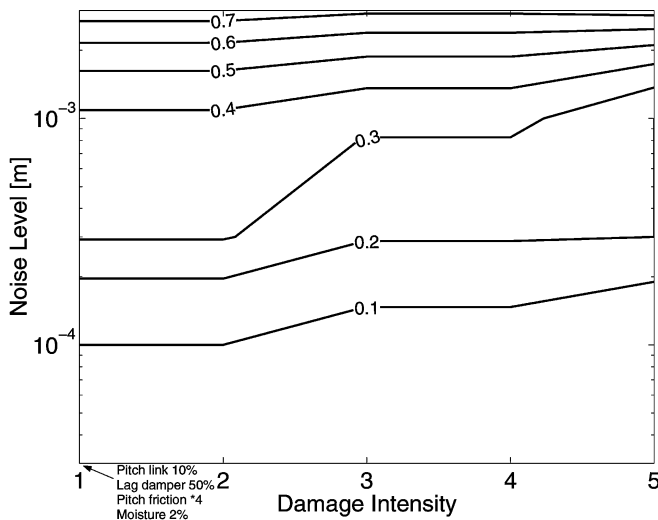


Fig. 7. False alarm rate.

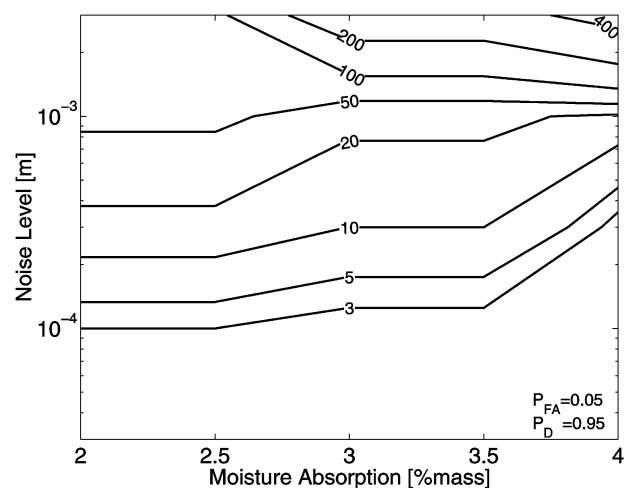
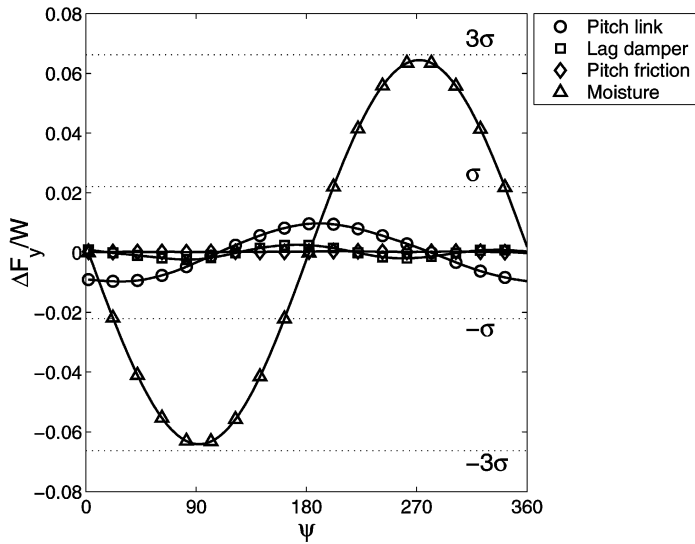
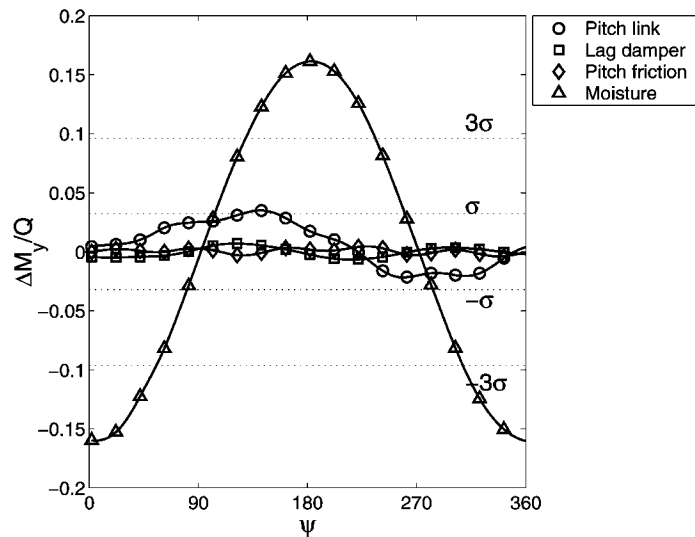


Fig. 9. Required number of runs to meet 0.05/0.95 false alarm/detection probabilities. Moisture absorption fault.



(a) Normalized lateral force differences $\Delta F_y/W$



(b) Normalized pitching moment differences $\Delta M_y/Q$

Fig. 10. Non-rotating hub load differences.

Moreover, during the decision time interval t_d , the probability results are quite decisive, suggesting that a Monte-Carlo analysis is not needed. The high probability values (≈ 1) indicates that the statistical experiment is also unnecessary.

Fuselage vibration measurements

Consider the same rotor as in the previous section. In this case also, only one damage level is considered, consisting of 5% stiffness reduction for the pitch link damage, 68% lag damping reduction, pitch friction which results in a pitch damping increase of factor 1.5 and 0.5% mass increase due to moisture absorption. The FDI algorithm is based on fuselage vibration measurements in trimmed forward flight. Vibration levels are measured in 3 locations on the fuselage (assumed to be rigid), where 2 directions are considered in each location: pilot seat—vertical and lateral directions, wing tip—vertical and longitudinal, and hub—lateral and longitudinal. Accelerometers are used as sensors, where the noise standard deviation, in this study, is 0.007g. Two vibration differences, measured at the pilot seat, are shown in Fig. 12, as an exam-

Table 2. Monte-Carlo FDI results

True Fault	Identified Fault	ID Probability
No damage	No damage	0.69
Pitch link damage	Pitch link damage	0.99
Lag damper damage	Lag damper damage	0.99
Pitch friction	Pitch friction	0.68
Moisture absorption	Moisture absorption	0.99

ple. Figure 12(a) demonstrates the vertical vibration differences (Δa_z) and Fig. 12(b) shows the lateral vibration differences (Δa_y), both measured in g. The moisture absorption case clearly results in larger differences, due to high vibration levels caused by the rotor mass imbalance. These large differences indicate high detectability for this type of fault. The pitch friction fault, as shown in Fig. 12, is expected to be less detectable since the vibration differences, caused by this type of fault, are quite small. This a priori statement is confirmed by the following results.

Table 2 summarizes Monte-Carlo results, which indicate good identification capability for the pitch link, lag damper and moisture absorption faults. The case of the pitch friction fault, as seen before in Fig. 12, is hard to detect due to the lack of sufficient vibration signature. Therefore, this fault model mixes with the undamaged baseline model, causing, on the one hand, detection problems, and, on the other, a relatively high false alarm rate. The same phenomenon was also observed with the lag damper fault detection based on blade tip response measurements.

Hub load measurements

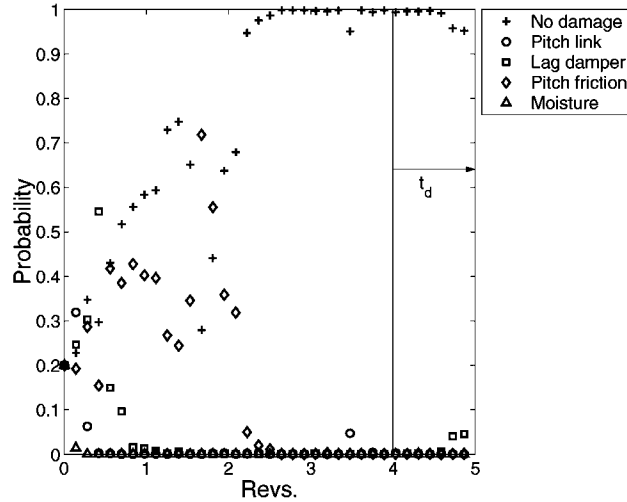
Consider a hingeless fixed shaft rotor with elastic blades, with the properties listed in Table 1. The blade beamwise and chordwise stiffnesses and torsional rigidity are $EI_b = 7.6 \times 10^4 \text{ Nm}^2$, $EI_c = 12 \times 10^5 \text{ Nm}^2$ and $GJ = 8.6 \times 10^4 \text{ Nm}^2$, respectively. The blade local damage, discussed in this section, is a crack at a specific location along the span. This crack is simulated by reducing the stiffnesses (bending stiffnesses and torsional rigidity) at a particular finite element in the blade structural model, as illustrated in Fig. 13. In this study, the damage intensity is modeled by a 5% stiffness reduction. Hub loads are measured with additive measurement noises having standard deviations of 1 kN and 1 kN-m for the force and moment measurements, respectively. Four filters are constructed, based on 4 models in which the damage location x , measured from the hub, assumes 4 discrete normalized values: $x/R = 0.15, 0.35, 0.55, 0.75$. The 5th filter simulates the undamaged case. The true damage, also simulated as a 5% stiffnesses reduction, occurs at the discrete locations $x/R = 0.1, 0.2, 0.3 \dots 0.9$. (Note that the true location is never identical to one of the modeled locations).

Figure 14 shows an example of the damaged case load differences with respect to the undamaged loads. As could be expected, damage located near the root results in the largest difference. As the damage location approaches the tip, the differences diminish.

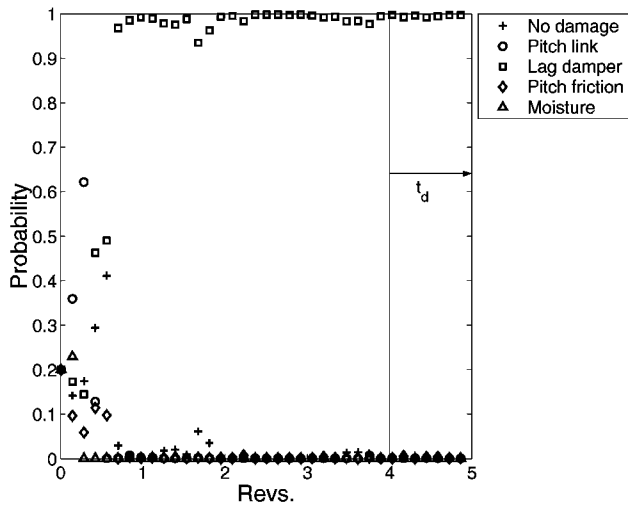
Table 3 summarizes Monte-Carlo results, which indicate good identification capabilities. In most cases, the model corresponding to damage location closest to the true location is indeed assigned the highest fitness probability. The case where the true damage occurs near the tip ($x/R = 0.9$) results in a missed detection. As can be expected, this case constitutes a very difficult problem and requires special treatment.

In passing, some remarks are in order concerning the use and implementability of the proposed new FDI method.

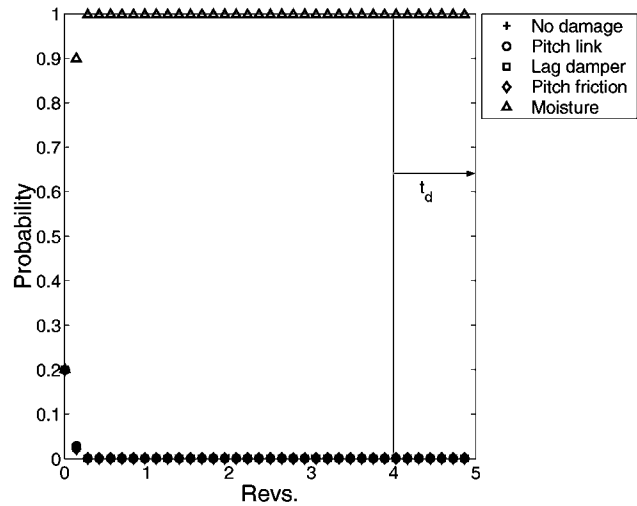
Remark 1. An important issue with all model-based methods is sensitivity to modeling uncertainties. In practice, it can be expected that



(a) No damage case



(b) Lag damper fault



(c) Moisture absorption fault

Fig. 11. Single-run identification probability time history. t_d is the inspection interval.

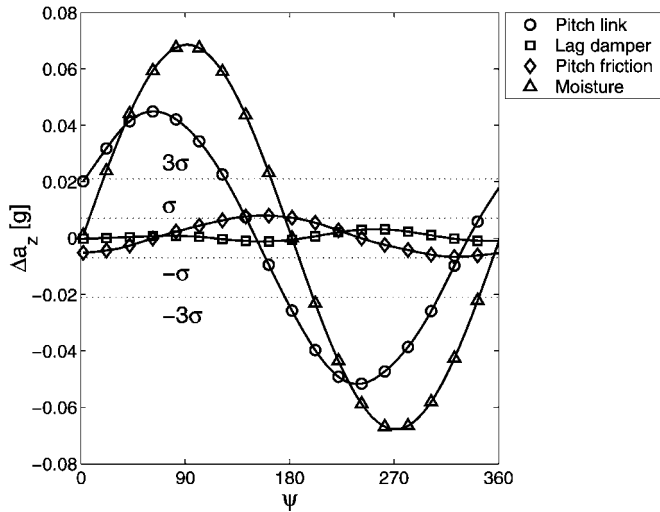
Table 3. Monte-Carlo identification results

True Damage Location	Identified Location	Identification Probability
No damage	No damage	0.99
0.1	0.15	0.99
0.2	0.15	0.99
0.3	0.35	0.91
0.4	0.35	0.89
0.5	0.55	0.63
0.6	0.55	0.99
0.7	0.75	0.99
0.8	0.75	0.97
0.9	No damage	0.90

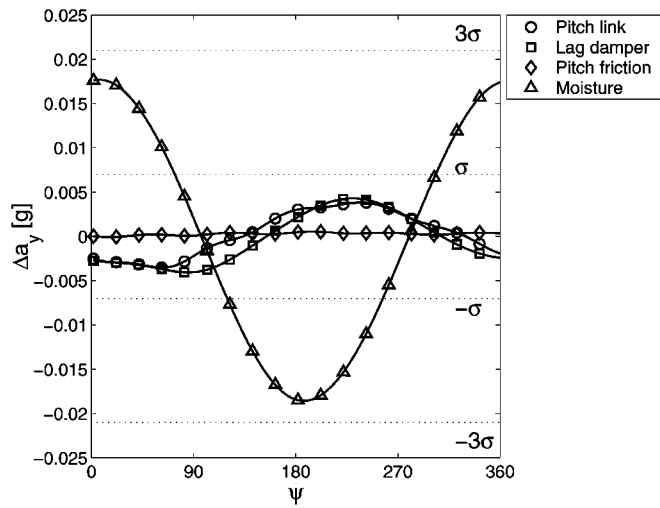
some variations will exist between (undamaged) production blades. This gives rise to the question of how well can the proposed method cope with structural modeling uncertainties. Recent results, presented in Ref. 18, show that the proposed FDI algorithm provides good performance even

when some variations are applied to some of the system parameters (up to 20% variation was implemented in the study presented in Ref. 18). These variations may also represent the case of undamaged, but slightly different blades.

Remark 2. In many recently published studies (Refs. 27–29), as well as in existing HUMS reports (Ref. 30), the measurement noise is treated through averaging. In the case of rotating machinery (as is the case of a helicopter rotor), the input signals are periodic, where the averaged cycle is calculated using all the response cycles up to a specific time point. Assuming the noise to have zero mean and variance σ^2 , combined with the assumption that the measurements are independent and identically distributed, the variance of the sample mean, denoted by $\bar{\sigma}^2$, decreases according to $\bar{\sigma}^2 = \sigma^2/N$, where N is the sample size. Therefore, as the number of cycles, used to calculate the average cycle, is increased, the noise level is decreased. Since noise is not treated inherently when filtering algorithms are not used, or in non-model based methods, this noise reduction technique is applicable. However, the averaging process introduces measurement correlation in time, since the averaged cycle depends upon all the previous signal cycles. This is contradictory to the

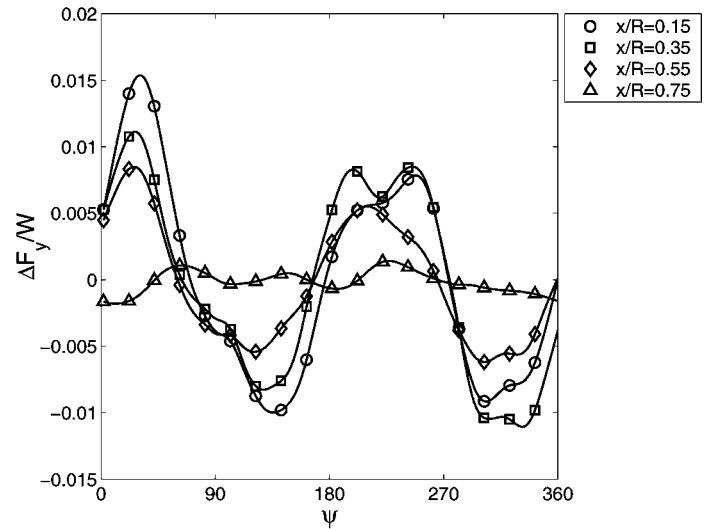


(a) Vertical vibration differences Δa_z

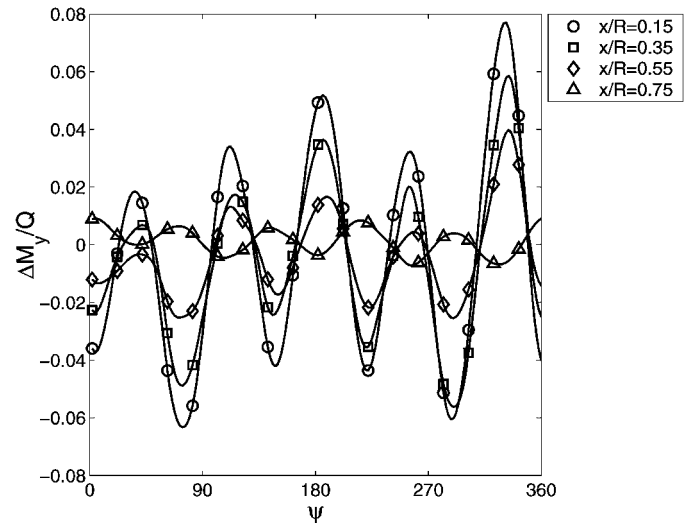


(b) Lateral vibration differences Δa_y

Fig. 12. Pilot seat vibration differences.



(a) Normalized lateral force differences $\Delta F_y/W$



(b) Normalized pitching moment differences $\Delta M_y/Q$

Fig. 14. Non-rotating hub load differences.

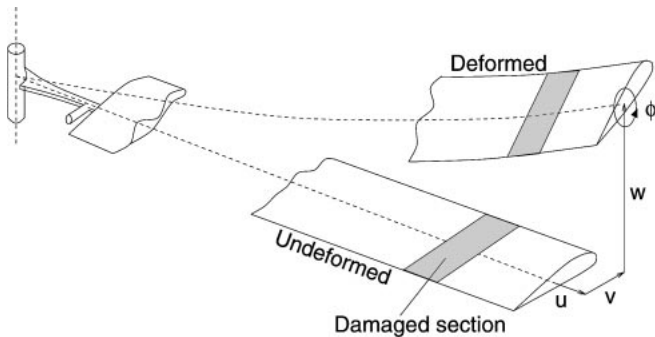


Fig. 13. A damaged elastic blade.

basic filtering assumption of white measurement noise. Hence, noise averaging cannot be implemented with filters without the use of proper techniques to deal with colored measurement noise (Ref. 31). Since the proposed MMAE approach uses model information to filter the noisy measurements, it is plausible that it should be able to decrease the estimation error variance much faster than the decrease rate of non-model based simple averaging, rendering the required number of cycles needed for correct damage identification significantly smaller.

Conclusions

A model-based damage detection algorithm for a helicopter rotor, using an adaptive estimation technique, incorporating noisy measurements, is presented. The coupled blade-fuselage dynamic behavior is introduced using the RAPID package where finite element model of the blade is utilized. A set of Kalman filters is constructed to simulate various rotor faults. The proposed method also enables sensors of various types to be implemented.

The algorithm presented constitutes a new approach towards damage detection in mechanical systems. Contrary to other model-based damage detection methods in helicopter rotors, such as methods based on neural networks, this approach requires no training stage. Moreover, the algorithm treats measurement and process noise inherently, accounting for the noisy rotor environment and modeling uncertainties. Combined with the model-based feature, the proposed algorithm eliminates the need for a training stage and enables a wide range of flight regimes. The damage detection capability is tested in various cases. In general, for low noise levels, this approach produces excellent results. The illustrative

rotor faults considered in this work demonstrate several levels of detectability. Pitch link damage was found to be highly detectable, for all sets of measurements considered. This emerges from the relatively high response sensitivity to pitch changes. On the contrary, lag damper damage was hard to detect using blade tip response measurements, since small damping values are present. Lag damping changes, in this case, have a small effect on the overall rotor response. The detectability of this type of damage was shown to increase significantly using hub load measurements. Pitch friction was hard to detect using fuselage vibrations, due to the lack of significant vibration signature. Blade moisture absorption detectability is also quite high. In cases of poor single-run performance, the suggested statistical experiment enables sustaining a low false alarm rate combined with a high detection capability. The case of a blade local stiffness defect was also investigated. It was shown that, using noisy hub load measurements, this approach is capable of detecting, and, in most cases, correctly locating small stiffness changes along the span.

The significant advantage of the proposed approach arises from the filtering process enabling probabilistic determination based on relatively little information. Introducing an external excitation in this case would probably increase damage detectability since the transient system response will provide additional information.

References

- ¹Linder, D. K., and Kirby, G., "Location and Estimation of Damage in a Beam Using Identification Algorithms," AIAA/SME Adaptive Structures Forum, Washington, D.C., April 21–22, 1994.
- ²Kahl, K., and Sirkis, J. S., "Damage Detection in Beam Structures Using Subspace Rotation Algorithm with Strain Data," *AIAA Journal*, Vol. 34, (12), December 1996, pp. 2609–2614.
- ³Ostachowicz, W. M., and Krawczuk, M., "Analysis of the Effect of Cracks on the Natural Frequencies of a Cantilever Beam," *Journal of Sound and Vibration*, Vol. 150, (2), 1991, pp. 191–201.
- ⁴Sundermeyer, J. N., and Weaver, R. L., "On Crack Identification and Characterization in a Beam by Non-Linear Vibration Analysis," *Journal of Sound and Vibration*, Vol. 183, (5), 1995, pp. 857–871.
- ⁵Yuen, M. M. F., "A Numerical Study of the Eigenparameters of a Damaged Cantilever," *Journal of Sound and Vibration*, Vol. 103, (3), 1985, pp. 301–310.
- ⁶Kiddy, J., and Pines, D., "Eigenstructure Assignment Technique for Damage Detection in Rotating Structure," *AIAA Journal*, Vol. 36, (9), September 1998, pp. 1680–1685.
- ⁷Kiddy, J., and Pines, D., "The Effects of Aerodynamic Damping on Damage Detection in Helicopter Main Rotor Blades," American Helicopter Society 54th Annual Forum Proceedings, Montreal, Canada, May 25–27, 1999.
- ⁸Ganguli, R., and Chopra, I., "Simulation of Helicopter Rotor-System Structural Damage, Blade Mistracking, Friction and Freeplay," *Journal of the American Helicopter Society*, Vol. 35, (4), July 1998, pp. 591–597.
- ⁹Stevens, P. W., Hall, D. L., and Smith, E. C., "A Multidisciplinary Research Approach to Rotorcraft Health and Usage Monitoring," American Helicopter Society 52nd Annual Forum Proceedings, Washington, D.C., June 4–6, 1996.
- ¹⁰Hass, D. J., and Schaefer, C. G., "Emerging Technologies for Rotor System Health Monitoring," American Helicopter Society 52nd Annual Forum Proceedings, Washington, D.C., June 4–6, 1996.
- ¹¹Ganguli, R., Chopra, I., and Hass, D. J., "A Physics Based Model for Rotor System Health Monitoring," 22nd European Rotorcraft Forum Proceedings, Brighton, UK, September 1996.
- ¹²Yang, M., Chopra, I., and Hass, D. J., "Rotor System Health Monitoring Using Coupled Rotor-Fuselage Vibration Analysis," American Helicopter Society 56th Annual Forum Proceedings, Virginia Beach, Virginia, May 2–4, 2000.
- ¹³Larden, B. D., "An Analysis of HUMS Vibration Diagnostic Capabilities," American Helicopter Society 53rd Annual Forum Proceedings, Virginia Beach, Virginia, April 29–May 1, 1997.
- ¹⁴Hess, R., Chaffee, M., Page, R., and Roseberry, K., "Realizing an Expandable Open HUMS Architecture," American Helicopter Society 56th Annual Forum Proceedings, Virginia Beach, Virginia, May 2–4, 2000.
- ¹⁵Hass, D. J., Baker, T., Sspracklen, D., and Schaefer, C., "Joint Advanced Health and Usage Monitoring System (JAHUMS) Advanced Concept Technology Demonstration (ACTD)," American Helicopter Society 56th Annual Forum Proceedings, Virginia Beach, Virginia, May 2–4, 2000.
- ¹⁶Robeson, E., "MH-47E Structural Usage Monitoring System (SUMS) Fleet Demonstration Results," American Helicopter Society 56th Annual Forum Proceedings, Virginia Beach, Virginia, May 2–4, 2000.
- ¹⁷Ghoshal, A., Harrison, J., Sundaresan, M. J., Schulz, M. J., and Pai, P. F., "Toward Development of an Intelligent Rotor System," American Helicopter Society 56th Annual Forum Proceedings, Virginia Beach, Virginia, May 2–4, 2000.
- ¹⁸Alkhahe, J., "Helicopter Faults, Simulation, Detection and Identification," Ph.D. thesis, Technion, Israel Institute of Technology, Haifa, Israel, March 2002.
- ¹⁹Alkhahe, J., Oshman, Y., and Rand, O., "Adaptive Estimation Methodology for Helicopter Blade Structural Damage Detection," *Journal of Guidance, Control and Dynamics*, Vol. 25, (6), November–December 2002, pp. 1049–1057.
- ²⁰Alkhahe, J., Rand, O., and Oshman, Y., "Damage Detection in a Helicopter Rotor by Adaptive Estimation," 26th European Rotorcraft Forum Proceedings, The Hague, The Netherlands, September 26–29, 2000.
- ²¹Alkhahe, J., Rand, O., and Oshman, Y., "Helicopter Rotor Health Monitoring Using Adaptive Estimation," American Helicopter Society 57th Annual Forum Proceedings, Washington, DC, May 9–11, 2001.
- ²²Magill, D. T., "Optimal Adaptive Estimation of Sampled Stochastic Processes," *IEEE Transactions on Automatic Control*, Vol. AC-10, (4), October 1965, pp. 434–439.
- ²³Maybeck, P. S., *Stochastic Models, Estimation, and Control*, Vol. 2, Academic Press, New York, 1982.
- ²⁴Stepaniac, M. J., and Maybeck, P. S., "MMAE-Based Control Redistribution Applied to the VISTA F-16," *IEEE Transactions on Aerospace and Electronic Systems*, Vol. 34, (4), October 1998, pp. 1249–1259.
- ²⁵Rand, O., "RAPID/Plus: Rotorcraft Analysis for Preliminary Design + Aeroelasticity: User Manual," Technical Report TAE-831, Technion, Israel Institute of Technology, Haifa, Israel, January 1999.
- ²⁶Freund, J. E., *Modern Elementary Statistics*, 6th edition, Prentice-Hall, Englewood Cliffs, NJ, 1984.
- ²⁷Stevens, P. W., and Smith, E. C., "Active Interrogation of Helicopter Rotor Faults Using Trailing Edge Flap Actuation," American Helicopter Society 57th Annual Forum Proceedings, Washington, D.C., May 9–11, 2001.
- ²⁸Samuel, P., and Pines, D., "Planetary Gear Box Diagnostics using Adaptive Vibration Signal Representation: A Proposed Methodology," American Helicopter Society 57th Annual Forum Proceedings, Washington, D.C., May 9–11, 2001.

²⁹Campbell, R., Garga, A., McClintic, K., Lebold, M., and Byington, C., "Pattern Recognition for Fault Classification with Helicopter Vibration Signals," American Helicopter Society 57th Annual Forum Proceedings, Washington, D.C., May 9–11, 2001.

³⁰Grabill, P., Berry, J., Grant, L., and Porter, J., "Automated Helicopter

Vibration Diagnostics for the US Army and National Guard," American Helicopter Society 57th Annual Forum Proceedings, Washington, D.C., May 9–11, 2001.

³¹Mendel, J. M., *Lessons in Digital Estimation Theory*, Prentice–Hall, Englewood Cliffs, NJ, 1987.